4-1-1997

Optimization of Plasmas for Recombination-Pumped Short-Wavelength Lasers

M. Murphy
Swarthmore College

C. Glasheen
Swarthmore College

F. A. Moscatelli
Swarthmore College

Thomas D. Donnelly
Harvey Mudd College

Optimization of plasmas for recombination-pumped short-wavelength lasers

M. Murphy, C. Glasheen, F. A. Moscatelli, and T. D. Donnelly
Department of Physics, Swarthmore College, Swarthmore, Pennsylvania 19081
(Received 18 November 1996)

We report on experiments investigating the optimization of laser-ablated plasmas which are used to produce recombination-pumped, short-wavelength lasers. We evaluate the density of electrons and neutral atoms in laser ablated lithium and carbon plasmas as a function of time and distance away from the ablated target surface. We use an interferometric technique which can reveal information about the temperature of the plasma electrons. We find that the cold electrons which result in gain in recombination-pumped lithium lasers on the Lyman-α transition are produced by the high-intensity pump pulse rather than the lower intensity ablating pulse. [S1050-2947(97)51604-0]

PACS number(s): 42.60.By, 52.50.Jm

Over the past decade there has been extensive effort to explore and develop short-wavelength lasers; Ref. [1] reviews of much of this work. The first soft x-ray laser was demonstrated in 1984 at Lawrence Livermore National Laboratory at a wavelength of 21 nm [2]. In this experiment the NOVA laser was used to create a plasma containing energetic free electron that collisionally pumped the laser transition. Since then, also using the NOVA laser, lasers have been demonstrated at wavelengths as short as 4.3 nm [3]. Following this original work, photoionization-pumped [4] and recombination-pumped [5] lasers were also demonstrated. In each of these experiments, a kilojoule of energy from the pump laser was required to produce the proper environment for the short-wavelength laser. Pump lasers with these large energies are not generally available and, in the past, the necessity of their use has limited the development of short-wavelength lasers to large research facilities.

Recently, however, high-intensity table-top lasers have made short-wavelength laser experiments more accessible. Using such a table-top system, a collisionally pumped laser has been demonstrated at 42 nm [6], and gain has been reported at 13 nm in a recombination-pumped scheme [7–10]. These experiments have demonstrated the downsizing of short-wavelength laser experiments to pump lasers with approximately 100 mJ of energy, an energy now achieved with commercially available high-intensity, short-pulse laser systems. The ability to use smaller pump lasers in these experiments will increase the use and eventual application of short-wavelength laser systems.

The gain reported in Refs. [7–10] was on the Lyman-α transition of Li^{2+}, and was demonstrated in the context of significant theoretical investigation of high-intensity, short pulse lasers as possible drivers for recombination pumped short-wavelength lasers (see, for example, [11,12]). These lasers are attractive as pumps because optical-field ionization (OFI) of atoms by these laser pulses can create high-charge-state, nonequilibrium plasmas with a propensity for recombination. The primary mode of recombination in these systems is three-body recombination, whose rate, R_{3B}, depends strongly on electron temperature T_e and electron density N_e: $R_{3B} \sim N_e^2 T_e^{9/2}$ [13]. OFI driven, recombination-pumped short-wavelength lasers have been proposed in plasmas of aluminum [14], carbon [14], and neon [15], to name a few. A common feature of these systems is that they require electron-ion recombination to occur on a time scale that is short compared to the natural lifetime of the laser transition, thus requiring a plasma with high electron density and cold electron temperature.

We set out to empirically determine how this OFI plasma can best be produced to achieve gain; we consider both lithium and carbon lasing media. Our considerations are motivated by the experiments described in Refs. [7–10], and the theoretical considerations found in Ref. [12]. Each of the above experiments produce a plasma appropriate for a recombination-pumped, short-wavelength laser in the following, two-step manner. First, a sample of lithium is ablated by a low-intensity pulse ($\sim 10^9$ W/cm^2 in Refs. [7,8], and $>10^{10}$ W/cm^2 in Refs. [9,10]) to produce a vapor of atoms, which is, in turn, used as a laser target. After some time delay, the ablating pulse is followed by a high-intensity pulse ($>10^{17}$ W/cm^2), which is capable of ionizing the lithium vapor atoms to the appropriate ionization stage (Li^{3+}). Under the proper conditions, the high-intensity pulse will produce a plasma which undergoes rapid three-body recombination, and subsequently lases. It is crucial that the three-body recombination occur quickly, so that the upper laser level ($n=2$) can be populated on a time scale which is short compared to the natural lifetime of the state (26 ps), otherwise the population inversion between the $n=1$ and $n=2$ states is spoiled. Again, this necessitates a cold, dense electron population, as can be seen from the dependencies of R_{3B}. Which of the above two pulses, the ablating pulse or the high-intensity pulse, produce these electrons, has been an open question. Since the operation of such a laser depends critically on the electrons, knowing the mechanism by which they are produced may allow optimization of the laser's performance. Further motivating our study, given the parameters of the ablating laser, hydrodynamic models have been unable to reproduce the characteristics of the ablated vapor as stated in Refs. [7–9].

In our investigation, we establish which of the two laser pulses is responsible for producing the cold electrons in the experiments of Ref. [7,8], and we further determine the density of the ablated plasma as function of both time and position off the target surface. With knowledge of the electron temperature and density, the most desirable experimental

conditions for realizing a recombination-pumped short-wavelength laser can be determined.

The optimal plasma conditions for gain occur with particular constraints on T_e and N_e. In the lithium system, for example, an electron density is required which is high enough to create a substantial population inversion (this is calculated to be $>10^{18}$ cm^{-3} [16]), yet is low enough to avoid collisional heating of the electrons via inverse-bremsstrahlung during the high-intensity pulse (less than approximately 10^{19} cm^{-3} [17]). Considerations of the electron temperature are twofold. If the electrons are produced by the ablating pulse, hydrodynamics will set the electron temperature as a function of time and distance away from the target surface. If, on the other hand, the electrons are produced by the high-intensity laser pulse, their temperature will result from energy imparted by the pulse during the OFI process. In this case, the temperature can be determined from models described in Ref. [11]. In either case, one would like to know the electron temperature and the mechanism by which it is established, to better control the lasing environment.

References [7–9] report some nonlinear growth of laser signal as a function of the length of the gain medium; this indicates that a population inversion is forming, and, therefore, it is believed that electrons of sufficiently low temperature are being produced. Reference [10] reports very strong evidence for lasing (gain-length GL$>$5), and further confirms the belief that cold electrons are produced. We find that for the conditions described in Refs. [7,8], the source of these cold electrons is not the low-intensity ablating laser.

The experimental methods we employ in our investigation follow that Ref. [18], and consist primarily of two-wavelength interferometry, plus absorption spectroscopy. A Mach-Zehnder interferometer was constructed with one beam passing through the laser-ablated vapor, at a variable distance from the target surface. An optical difference between this beam and the reference beam accrues due to changes in the index of the ablated vapor. These phases differences result from the presence of neutral atoms and free electrons. We assume the contribution due to the ions is small because their polarizability is significantly less than that of the neutral species, and because their density is small compared to that of the neutrals (see below). The optical phase difference $\Delta\phi$ between reference and probe beams, for light of wavelength λ, is given by $\Delta\phi = 2\pi L(n-1)/\lambda$, where L is the length of the medium whose index of refraction is n. The index of refraction of the plasma is

$$n \cong 1 + 2\pi(N_0\alpha_0 + N_e\alpha_e), \tag{1}$$

where N_0 and N_e are, respectively, the neutral atom and electron densities, and we assume that the second term on the right-hand side of the equation is small compared to unity. The polarizabilities α_0 and α_e are wavelength dependent. The electron polarizability is obtained through a classical treatment of the electron in an electromagnetic field of frequency ω, while the corresponding value for the atomic polarizability comes from a Lorentzian line-shape correction of the DC value, $\alpha_0(0)$, around the atom's principal resonant transition of frequency ω_0 [19]. In our analysis we take $\alpha_e(\omega) = e^2/(m\omega^2)$, and $\alpha_0(\omega) = \alpha_0(0)E_r^2/(E_r^2 - E_\omega^2)$, where E_r is the transition energy of the nearest dipole-allowed transition, E_ω is the photon energy, and both polarizabilities are in units of cm^{-3}. The relevant lithium transition is 1.85 eV above the ground state, and for carbon it is 5 eV above the ground state. The experimentally determined dc polarizabilities of lithium and carbon are, respectively, 12×10^{-24} cm^{-3} and 1.5×10^{-24} cm^{-3} [20].

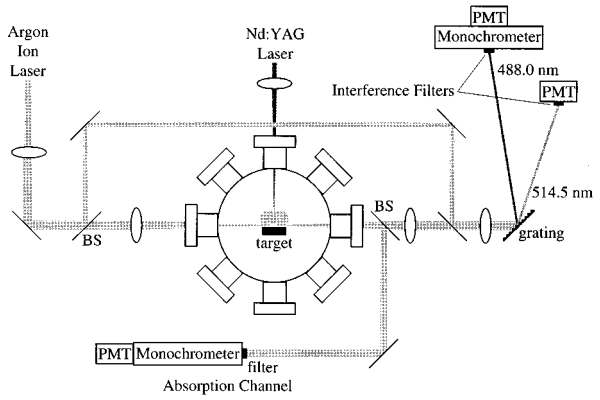

FIG. 1. Diagram of the experimental setup.

From our raw date, which consists of the intensity transmitted through the interferometer as a function of time, we extract the fringe shift function S. Since $S = \Delta\phi/2\pi$,

$$\lambda S(t) = 2\pi L[N_0(t)\alpha_0 + N_e(t)\alpha_e]. \tag{2}$$

To solve for both the electron and neutral atom densities from this single equation is, of course, impossible using a single probe wavelength; therefore, data is collected at two wavelengths. We use the two strongest lines of an argon-ion laser operating at 2 W: $\lambda_1 = 514.5$ nm and $\lambda_2 = 488$ nm.

The Mach-Zehnder interferometer was constructed with one beam arm, focused to a diameter of 20 μm directed through our vacuum chamber and passing at a variable distance from the target surface (see Fig. 1). The vacuum chamber is evacuated to 10^{-5} Torr. The target material was held on a stage that could be ''raster scanned'' to fresh spots for each ablation shot. The ablation pulse was produced by a Q-switched, frequency-doubled (532 nm) neodymium-doped yttrium aluminum garnet (Nd:YAG) laser operating with 200-mJ pulse energy, and 10-ns pulse duration. The Nd:YAG pulse was focused by a 25-cm focal-length cylindrical lens onto the target. Measurement of the focused beam showed that a 130-μm line focus was achieved over a 2-mm length. An abrupt edge of the line focus was produced on target using an imaging system and horizontal slits. These values yield 8×10^9 W/cm^2 as our maximum intensity of target. The intensity was varied during data collection using neutral density filters.

Although none of the lithium laser investigations referenced above use a Nd:YAG as an ablating laser, we believe that our results are applicable to a variety of experimental setups. In the intensity range of interest, the temperature of the ablated plasma is relatively insensitive to the wavelength and the duration of the ablating pulse. Over the intensity range of 10^8–10^{13} W/cm^2, temperatures of laser ablated plasmas vary by only a factor of 10 (see Table 4.2 of Ref. [22]); this has been demonstrated using a wide range of target materials. For nanosecond duration ablating pulses,

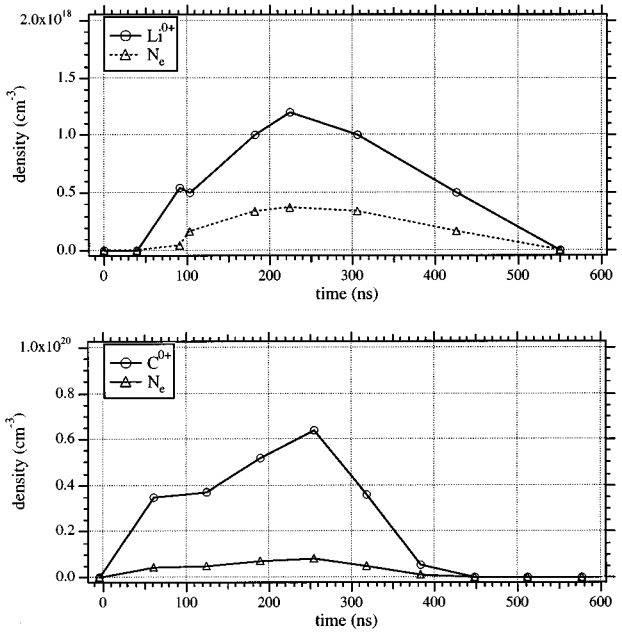

FIG. 2. Electron and neutral atom densities as a function of time measured for lithium and carbon targets. Lithium data: intensity of ablating laser pulse on target is 3×10^8 W/cm^2; probe beam is 250 μm from the target surface. Carbon data: intensity of ablating pulse on target is 1×10^9 W/cm^2; probe beam is 0 μm from the target surface.

plasma density will grow until the electron density is high enough to reflect the incoming pulse [22]. This occurs when the laser frequency is equal to the plasma frequency, and therefore the final density should vary with the square of the laser frequency. Since the frequency of our pulse is within a factor of 2 of those used in Refs. [7] and [8], and is of nearly the same duration (Ref. [7] uses a 20-ns pulse with $\omega = 7.6\times10^{15}$ Hz, and Ref. [8] uses a 10-ns pulse with $\omega = 6.1\times10^{15}$ Hz), we expect to create comparable plasmas. Plasmas of similar temperature and density will evolve similarly due to hydrodynamics.

In our setup, the argon-ion laser was operated in the all-lines mode so that five different lasing wavelengths were present in the probe beam. The green (514.5 nm) and blue (488 nm) lines were spatially separated in the beam with a diffraction grating placed after the interferometer. The central interference fringe was then directed through a interference filter (bandpass=3 nm) to a photomultiplier for detection. The signal-to-noise ratio of the interference fringes at 488 nm was lower than that at 514.5 nm. To improve this situation, we further discriminate the 488-nm fringe signal from the noise by sending it through a monochrometer before it reaches the photomultiplier.

Data was collected for carbon and lithium targets over intensities ranging from 8×10^9 W/cm^2 down to one hundredth that value, at four different positions above the target surface: 750, 500, 250, and 0 μm. In Fig. 2, we show some of the electron and neutral atom densities that are derived from the fringe shift data (corrected for absorption of the probe beam in the plasma); we estimate the uncertainty in the density values to be as large as 50% as a result of the noise on the interference fringes. Several features are noticeable. For both lithium and carbon targets it can be seen that no relevant density of free electrons is present after 550 ns. This indicates that in the experiments described in Refs. [7,8], at the time the high-intensity pump-pulse arrives (approximately 750 ns after the ablating pulse), only a fractionally ionized plasma or a neutral atomic vapor is present (see Fig. 2).

The carbon data was obtained for a higher ablating laser intensity than was used for the lithium data shown, and a correspondingly higher atomic density is observed. The observed density is similar to that required for the operation of a C^{5+}, recombination-pumped, laser operating at 18 nm [12]. The lithium result, which was obtained for a probe beam distance 250 μm from the target surface, shows a time delay between the ablating pulse ($t=0$) and the arrival of the plume. This delay is set by the hydrodynamic expansion of the plume, and indicates an expansion energy of approximately 1 eV, which is consistent with previous experimental results (see Table 4.2 in Ref. [22]).

An important point is that both the lithium and carbon targets produce only a fractionally ionized plasma (at the peak of the neutral density in Fig. 2, carbon is 10% ionized and lithium is 25% ionized). Thus, if this plasma were the sole source of the cold electrons, there would not be enough of them present to produce gain through recombination with the highly stripped ions which are produced by the high-intensity pulse. (One of the authors has shown this in calculations which relate electron density and gain under a variety of conditions [16]). Therefore, our laser-ablated plasma is incapable of providing the cold electrons that are critical for the operation of the short-wavelength laser. Since the ablating laser is not able to provide these electrons, the cold electrons must, in practice, be produced by the high-intensity pump pulse. This also explains a perplexing aspect of the data reported in Ref. [16]. They report an electron density of 2×10^{17} cm^{-3} in their ablated plasma, based on emission spectroscopy studies. They assume that this is also the electron density that accounts for the rapid recombination in the highly ionized plasma, and, therefore, is responsible for the gain they observe. This electron density is, however, thought to be too low [16], by approximately a factor of 10, to account for the high gain that they report. We can now offer an explanation of these seemingly contradictory results. Nagata *et al.* treat their ablated plasma as fully, singly ionized, and thus the source of cold electrons. Our results suggest that Nagata's plasma is *partially* ionized, having the reported electron density, but a much higher neutral atom density. Therefore, when the high-intensity pulse irradiates this plasma a significantly higher electron density is produced than that which was reported (perhaps above the 10^{18} cm^{-3} required for gain). It is this plasma which results in the observed population inversion and, thus, explains how it was possible for their system to generate the observed gain. In short, the high, neutral-atom density is produced by the ablating laser. The particular atom density above the target surface at a given time is determined by the intensity of this pulse on target and the ensuing hydrodynamics. The high-intensity pump pulse then generates the ion density, and produces the first cold free electron by multiphoton ionization on its leading temporal edge.

Finally, if the high-intensity pump pulse is responsible for providing the cold electrons, it is implicit that neither

inverse-bremsstrahlung, nor ponderomotive heating of the electrons during the high-intensity pulse, is sufficient to preclude the rapid formation of a population inversion.

We are currently improving our detection system to reduce the noise on our interference fringe signals. These improvements will allow us to do a more detailed study of the density-time-position phase-space of the ablated plasma. We will also be able to determine the temperature of the electrons produced by the ablating laser as a function of time and position above the target by measuring the absorption of a light beam traversing the ablated vapor. This absorption does not arise from the familiar mechanism of resonant transitions between discrete atomic states, but from inverse bremsstrahlung. We pick off a portion of the laser beam (see Fig. 1) that traverses the vapor and extract the optical thickness, τ, from the incoming and outgoing intensities, I_0 and I, respectively. From Beer's law, $I(\omega)=I_0\exp[-\tau(\omega)]$. The optical thickness can be related to the inverse bremsstrahlung absorption cross section to obtain the following expression for τ [21]:

$$\tau \cong 9.93\times 10^{-38}\frac{LN_e^2T_e^{-1/2}}{(\hbar\omega)^2}\left[\exp\left(\frac{\hbar\omega}{T_e}\right)-1\right], \qquad (3)$$

where temperature is measured in eV, density in cm^{-3}, and ω is the laser frequency. Thus, from a measurement of the absorption and our knowledge of N_e, we can obtain the electron temperature. In our continuing studies, we will determine the best time delay between the ablating and high-intensity pulses and the position above the target surface at which the high-intensity probe should be incident to optimize the production of a short wavelength, recombination-pumped laser in lithium or carbon.

In summary, we have used a two-color interferometry technique to show that the electrons that are critical for the operation of the lithium laser are produced by the high-intensity pump pulse. This implies that electrons produced by multiphoton ionization are cold enough to form a population inversion on the Lyman-α transition of lithium. We have also given an explanation of earlier seemingly contradictory results concerning electron density and gain in the lithium system.

We wish to acknowledge Carl Grossman for use of the Nd:YAG laser, Carr Everbach for the use of his oscilloscope, the technical assistance of Steven Palmer and John Dougherty, and the assistance of Walter Luh and Gabe Benjamin-Fernandez.

[1] R. C. Elton, *X-ray Lasers* (Academic, San Diego, 1990).
[2] D. L. Matthews *et al.*, Phys. Rev. Lett. **54**, 110 (1985).
[3] B. J. MacGowan *et al.*, Phys. Rev. Lett. **65**, 420 (1990).
[4] H. Kapteyn, R. W. Lee, and R. W. Falcone, Phys. Rev. Lett. **57**, 2939 (1986).
[5] S. Suckewer *et al.*, Phys. Rev. Lett. **54**, 1753 (1985).
[6] B. E. Lemoff *et al.*, Phys. Rev. Lett. **74**, 1574 (1995).
[7] Y. Nagata *et al.*, Phys. Rev. Lett. **71**, 3774 (1993).
[8] T. D. Donnelly *et al.*, J. Opt. Soc. Am. B **13**, 185 (1996).
[9] K. M. Krushelnick, W. Tighe, and S. Suckewer, J. Opt. Soc. Am. B **13**, 306 (1996).
[10] D. V. Korobkin *et al.*, Phys. Rev. Lett. **77**, 5206 (1996).
[11] P. B. Corkum, N. H. Burnett, and F. Brunel, Phys. Rev. Lett. **62**, 1259 (1989).
[12] N. H. Burnett and P. B. Corkum, J. Opt. Soc. Am. B **6**, 1195 (1989).
[13] Y. Zel'Dovich and Y. Raizer, *Physics of Shock Waves and High-Temperature Hydrodynamic Phenomena* (Academic, New York, 1966).
[14] N. H. Burnett and G. D. Enright, IEEE J. Quantum Electron. **26**, 1797 (1990).
[15] D. C. Eder, P. Amendt, and S. C. Wilks, Phys. Rev. A **45**, 6761 (1992).
[16] T. D. Donnelly, R. W. Lee, and R. W. Falcone, Phys. Rev. A **54**, R2691 (1995).
[17] T. Ditmire, Phys. Rev. E **54**, 6735 (1996).
[18] C. D. David, Appl. Phys. Lett. **11**, 394 (1967).
[19] W. Demtroeder, *Laser Spectroscopy*, 2nd ed. (Springer-Verlag, Berlin, 1996); H. Griem, *Plasma Spectroscopy* (McGraw-Hill, New York, 1964).
[20] E. M. Purcell, *Electricity and Magnetism* (McGraw-Hill, New York, 1985).
[21] C. D. David and H. Weichel, J. Appl. Chem. **40**, 3674 (1969).
[22] J. F. Ready, *Effects of High-Power Laser Radiation* (Academic, New York, 1971).